Molecular treatment of electron capture at low to intermediate collision energies: Collisions of B^{4+} ions with H atoms

N. Shimakura
General Education Department, Niigata University, Niigata 950-21, Japan

S. Suzuki
Department of Chemistry, Faculty of Science, Niigata University, Niigata 950-21, Japan

M. Kimura
Argonne National Laboratory, Argonne, Illinois 60439
and Department of Physics, Rice University, Houston, Texas 77251

(Received 8 September 1992)

Partial and total cross sections for electron capture in collisions of B^{4+} ions with H atoms from 100 meV/amu to 10 keV/amu have been rigorously determined by using the molecular-orbital expansion method modified by the inclusion of electron translation factors. Quantum-mechanical (3 channels) and semiclassical (12 channels) methods have been employed at collision energies lower than 30 eV/amu and higher than 15 eV/amu, respectively. The agreement of the present results with measurements above 1 keV/amu is reasonable. In our cross sections for the singlet manifold, rather large oscillatory structures are found below 10 eV/amu that are attributable to Stueckelberg-type oscillation. At collision energies below a few eV/amu, the $B^{3+}(1s3d)$ and $B^{3+}(1s3p)$ states are the dominant states for the triplet and singlet manifolds, respectively. However, the $B^{3+}(1s3p)$ state for the triplet and $B^{3+}(1s3d)$ state for the singlet take over above these energies. At energies above 1 keV/amu, three states, the $B^{3+}(1s3s)$, $B^{3+}(1s3p)$, and $B^{3+}(1s3d)$ states, contribute equally to the electron-capture process. A comparison of the present B^{4+} results with previous results for different projectiles with the same charge (i.e., Be^{4+}, C^{4+}, and N^{4+}) reveals that although the cross sections of all these systems lie roughly within a certain range of magnitudes at intermediate collision energies ($E=0.5$–10 keV/amu), differences begin to emerge in magnitude and energy dependence below this energy. We examined the scalability of the cross section; some remarks on the scaling are given.

PACS number(s): 34.10.+x, 34.20.−b, 34.70.+e

I. INTRODUCTION

An accurate determination of the cross sections and an understanding of the dynamics of the electron-capture process by multiply charged ions from hydrogen atoms over a wide range of collision energies are important in studies in a variety of subfields of sciences, particularly fusion plasma and astrophysics. In these fields, cross-section data for all processes from the meV region to the MeV region are essential for models that simulate relevant physical environments, as well as for analysis of the spectroscopic data obtained.

In our continuing effort to study collisions of multiply charged ions, we have carried out a systematic study of the electron-capture process for projectiles whose charges are five (i.e., N^{5+}[1], C^{5+}[2], and O^{5+}[3]) and four (i.e., N^{4+}[4]). In this paper, electron capture from H atoms by B^{4+} ions is studied in the energy range from 100 meV/amu to 10 keV/amu. Our theoretical approach is a molecular-orbital-expansion method modified by atomic-type electron translation factors (ETF's). Coupled equations are solved in both the quantum-mechanical and semiclassical representations. This ($B^{4+}+H$) system has attracted increasing attention, particularly from groups studying fusion, because B^{4+} ions, as one of the impurities in fusion plasma, are known to play a crucial role in cooling in a fusion reactor [5]. Because no rigorous theoretical study has been conducted on the system, a set of cross sections and guidelines for application are urgently needed. Three experimental results for electron capture above 1 keV/amu have been reported by Crandall, Phaneuf, and Meyer [6], Goffe, Shah, and Gilbody [7], and Gardner *et al.* [8]. However, their values are rather widely scattered, from 25×10^{-16} cm^2 to 50×10^{-16} cm^2 in the range 2–10 keV/amu.

In a previous paper [2], we compared our cross sections for the electron-capture process from H atoms by C^{5+} ions with those for other ions having projectile charge $Z_p=5$ (i.e., B^{5+} and N^{5+} ions). In extending the previous study, we now intend to investigate the effects of core electrons on electron capture from H atoms by ions having the same charge ($Z_p=4$) as B^{4+} ions. We also examine a scaling form for the cross sections proposed.

II. FORMULATION

Since the details of the method used in this paper have been described previously [9–11], only a brief summary of the basic technique and the specific information used for the calculation are given here.

A. Molecular states

The molecular electronic states are obtained by using a valence-bond configuration-interaction method. We describe molecular electronic wave functions as a linear combination of Slater determinants, and Slater-type orbitals (STO's) are used as a basis set. The orbital exponents of the STO's used in the calculation are given in Table I. The values for the B^{4+} and B^{3+} ions were obtained by variationally optimizing the energies of ionic levels. The values of the hydrogen atom were taken from the previous work of Sato *et al.* [12]. The accuracy of the present energy levels with respect to the experiment energies is better than 0.065%, except for the $B^{3+}(1s^2)$ level (0.16%) as compared in Table II with the spectroscopic values [13]. The difference in the $B^{3+}(1s^2)$ level appears to be somewhat large. However, this state is completely excluded from our close-coupling calculations because it was found to play no role in the electron-capture process in the present energy regime. In the triplet manifold, both the calculated and spectroscopic values are in the natural order, but this is not the case in the single manifold. In the singlet manifold the $B^{3+}(1s3s)$ state is the lowest level in the $B^{3+}(1s3l)$ manifold, but the second and the third levels are the $B^{3+}(1s3d)$ and $B^{3+}(1s3p)$ states, respectively. Similarly, in the $B^{3+}(1s4l)$ manifold, the $B^{3+}(1s4s)$, $B^{3+}(1s4f)$, $B^{3+}(1s4d)$, and $B^{3+}(1s4p)$ states have successively increasing energy. The presence of the reverse order of energy levels has been known for other atomic systems [14] and the cause is attributed to a weakening exchange effect between $1s$ and nlm electrons as l increases, resulting in a reversed order, for example, between the $1s3p$ and $1s3d$ levels. The order of these levels found in our calculation is consistent with the spectroscopic data [13,15].

TABLE I. Orbital exponents of the Slater-type orbital basis function.

B^{4+} and B^{3+}			H	
	Exponent			
Orbital	Triplet	Singlet	Orbital	Exponent
$1s$	6.000 00	6.000 00	$1s$	2.0
	5.000 00	5.000 00		1.0
	2.500 00	2.500 00		0.5
$2s$	2.989 31	3.196 70	$2s$	0.5
	1.494 65	2.007 90	$2p$	1.0
$2p$	2.879 58	1.893 75		0.5
	1.439 78	1.592 25		
$3s$	1.381 16	1.138 22		
$3p$	1.349 44	1.306 11		
$3d$	1.332 44	1.330 54		
$4s$	1.095 06	0.824 26		
$4p$	1.009 46	0.901 32		
$4d$	0.997 20	0.901 48		
$4f$	0.997 90	0.984 14		
$5s$	0.808 95	0.770 43		

TABLE II. Calculated and spectroscopic values of energy levels of $B^{3+}(1snl)$ ion (a.u.).

nl	Experiment [13]	Calculation	ΔE
	Triplet system		
$2s$	−14.737 96	−14.732 04	0.0059
$2p$	−14.576 69	−14.569 76	0.0069
$3s$	−13.457 65	−13.453 20	0.0044
$3p$	−13.414 36	−13.409 95	0.0044
$3d$	−13.391 58	−13.389 21	0.0023
$4s$	−13.029 72	−13.027 57	0.0022
$4p$	−13.013 40	−13.007 40	0.0060
$4d$	−13.001 10	−13.000 10	0.0009
$4f$	−13.001 83	−12.991 38	0.0104
	Singlet system		
$1s$	−22.034 96	−22.000 65	0.0343
$2s$	−14.583 06	−14.573 61	0.0094
$2p$	−14.480 45	−14.471 76	0.0086
$3s$	−13.415 15	−13.410 56	0.0046
$3d$	−13.391 58	−13.388 73	0.0028
$3p$	−13.386 20	−13.381 07	0.0051
$4s$		−13.009 16	
$4f$	−13.002 92	−13.001 08	0.0018
$4d$	−13.001 11	−12.998 70	0.0024
$4p$	−13.000 87	−12.995 80	0.0051
$B^{4+}(1s)+H(1s)$	−13.002 82	−13.000 01	0.0028

B. Collision dynamics

The three-channel quantum-mechanical close-coupling method was used at collision energies of 10^{-1}–25 eV/amu. The channels included are Σ states that asymptotically correlate with the $[B^{3+}(1s3p)+H^+]$, $[B^{3+}(1s3d)+H^+]$, and initial $[B^{4+}(1s)+H]$ states for both the triplet and singlet manifolds, because these states are found to be the dominant contributors to electron capture below 100 eV/amu. At the energies of 0.015–10 keV/amu, the twelve-channel semiclassical close-coupling method was employed. Those channels consist of seven Σ, four Π, and one Δ state from the initial, $B^{3+}(1s4s)$, $B^{3+}(1s4p)$ (for triplet), $B^{3+}(1s4f)$ (for singlet), and all $B^{3+}(1snl$, $n=2$ and 3) manifolds listed in Table II. As described in our previous papers [1,2,4], we used both straight-line and repulsive Coulomb trajectories for heavy-particle motion in order to examine the trajectory effect on the transition probabilities.

III. RESULTS

A. Adiabatic potentials and couplings

Adiabatic potential energies for the triplet and singlet manifolds of the BH^{4+} system are presented in Figs. 1(a) and 1(b) (Σ states only), respectively. These figures indicate that the initial channel and the $B^{3+}(1s3l)$ manifold possess strong avoided crossings at $R\sim 8$ a.u., which is considered to be the optimum location for transition (the reaction window) based on the Landau-Zener model [11].

Hence, electron capture to $B^{3+}(1s3l)$ states may be dominant at low to intermediate collision energies.

For the triplet manifold, three apparent avoided crossings occur at about 7.93 ($=R_1$), 4.40 ($=R_5$), and 2.45 a.u. ($=R_6$), with energy splittings of about 2.82×10^{-3}, 2.04×10^{-3}, and 2.50×10^{-2} a.u., respectively. Some other broad avoided crossings can be seen at $R=5.0-8.0$ a.u. among the 3Σ, 4Σ, 5Σ, and 6Σ states. The $B^{3+}(1s2l)$ states are expected to contribute to electron capture only at higher collision energies. In Fig. 1(a), only the 7Σ state is shown from the $B^{3+}(1s4l)$ manifold. This state and one Π state are included in the close-coupling calculations and asymptotically correlate to the $[B^{3+}(1s4s)+H^+]$ and $[B^{3+}(1s4p)+H^+]$ states, respectively. Our scattering results indicate that the contributions of these states to electron capture are insignificant (see Sec. III B 1).

For the singlet manifold, the lowest Σ state $[B^{3+}(1s^2)+H^+]$ is not displayed in Fig. 1(b) because it lies far below the other states shown. The general features of the potential energies of the singlet manifold are similar to those of the triplet manifold, but in this case five apparently avoided crossings occur at about 8.32 ($=R_1$), 7.62 ($=R_2$), 5.25 ($=R_4$), 4.28 ($=R_5$), and 2.48 a.u. ($=R_6$), with energy splittings of about 5.00×10^{-3}, 9.49×10^{-3}, 1.43×10^{-2}, 1.90×10^{-2}, and 1.27×10^{-2} a.u., respectively. For the singlet manifold, in addition to these avoided crossings, a broad avoided crossing can also be seen at about $R=7-8$ a.u., between the 4Σ and 5Σ states. Furthermore, the positions of two curve crossings at R_1 and R_5 in the singlet manifold are at much larger R and at smaller R, respectively, than those in the triplet manifold. This finding occurs because the asymptotic energies of the $B^{3+}(1s3l)$ states for the singlet manifold are higher than those for the triplet manifold relative to the initial state. These differences in the adiabatic potentials apparently cause the difference in electron-capture dynamics between the triplet and singlet manifolds.

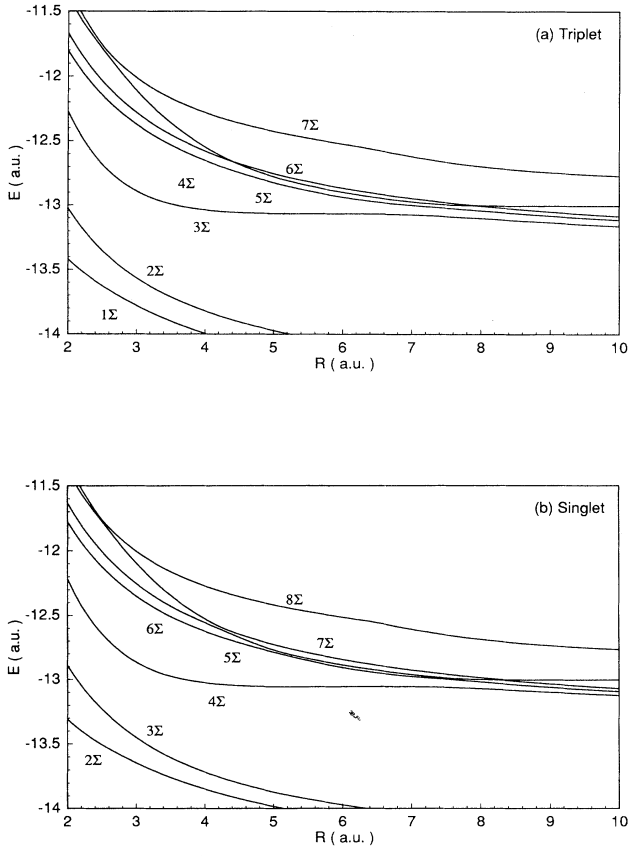

FIG. 1. Adiabatic potential energies for the BH^{4+} system. Only Σ states are shown for simplicity. (a) Triplet 1Σ, $B^{3+}(1s2s)+H^+$; 2Σ and 1Π, $B^{3+}(1s2p)+H^+$; 3Σ, $B^{3+}(1s3s)+H^+$; 4Σ and 2Π, $B^{3+}(1s3p)+H^+$; 5Σ, 3Π, and 1Δ, $B^{3+}(1s3d)+H^+$; 6Σ, $B^{4+}(1s)+H$; 7Σ, $B^{3+}(1s4s)+H^+$. (b) Singlet 2Σ, $B^{3+}(1s2s)+H^+$; 3Σ and 1Π, $B^{3+}(1s2p)+H^+$; 4Σ, $B^{3+}(1s3s)+H^+$; 5Σ, 2Π and 1Δ, $B^{3+}(1s3d)+H^+$; 6Σ, and 3Π, $B^{3+}(1s3p)+H^+$; 7Σ, $B^{4+}(1s)+H$; 8Σ, $B^{3+}(1s4s)+H^+$; 4Π, $B^{3+}(1s4f)+H^+$.

The radial and rotational coupling matrix elements (with atomic-type ETF's to the first order in velocity) necessary to solve the coupled equations were calculated. The representative results of these couplings are displayed in Fig. 2 for both the triplet and singlet manifolds. The couplings responsible for flux exit possess sharp peaks in the 7.9 a.u. (triplet manifold) and the 8.3 a.u. (singlet manifold), as discussed above, and similar sharp peaks in other couplings are seen for other avoided crossings, as expected.

B. Cross section and core electron effect

1. *Triplet manifold*

The present partial and total cross sections for the triplet manifold are shown in Fig. 3. The cross sections of the $B^{3+}(1s2s)$, $B^{3+}(1s2p)$, $B^{3+}(1s4s)$, and $B^{3+}(1s4p)$ states are not shown, because their values are negligibly small at all collision energies. The states lying above the $B^{3+}(1s4p)$ state are neglected for the triplet [or $B^{3+}(1s4f)$ for singlet] manifold in the close-coupling cal-

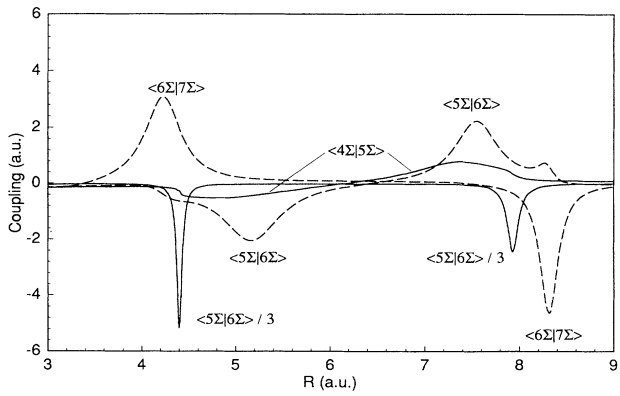

FIG. 2. Representative radial couplings for the triplet and singlet manifolds. Solid line, triplet; dashed line, singlet.

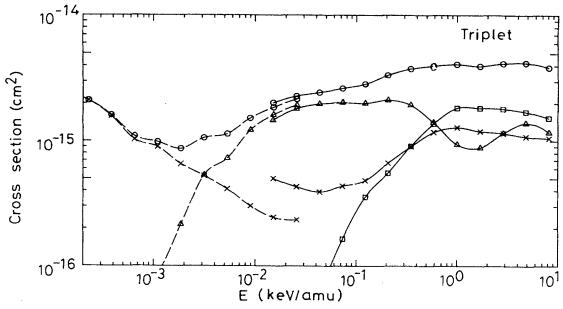

FIG. 3. Collision energy dependence of the total and partial electron-capture cross sections for the triplet manifold. The solid curve represents semiclassical results for the straight-line trajectory. The broken curve represents the quantum-mechanical results. ○, total; □, $B^{3+}(1s3s)+H^+$; Δ, $B^{3+}(1s3p)+H^+$; ×, $B^{3+}(1s3d)+H^+$.

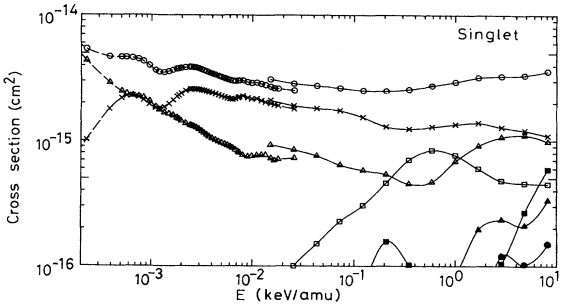

FIG. 4. Collision energy dependence of the total and partial electron-capture cross sections for the singlet manifold. The symbols ○, □, △, are the same as in Fig. 3. New symbols are ■, $B^{3+}(1s4s)$; ▲, $B^{3+}(1s4f)$; ●, $B^{3+}(1s2p)$.

culations. The contribution of the higher states is considered to be quite small, because the flux is transferred to these states via the $[B^{3+}(1s4s)+H^+]$ state as an intermediate state, and the contribution of this intermediate state itself is negligibly small. Figure 3 indicates that the $B^{3+}(1s3l)$ manifold clearly dominates electron capture in the entire energy region. At higher collision energies, three states [$B^{3+}(1s3s)$, $B^{3+}(1s3p)$, and $B^{3+}(1s3d)$] contribute equally to electron capture. At intermediate energies, below 0.5 keV/amu, the $B^{3+}(1s3p)$ state becomes the main contributor to the electron-capture process. At still low energies, below 3 eV/amu, the $B^{3+}(1s3d)$ state again plays a dominant role. These observations are expected from the analysis of the potential energies and radial couplings.

A collision history study (not shown) suggests that at high energies, at R_1 and R_2 (7.3 a.u.) where the energy splitting is very small and the corresponding radial coupling is strong and sharp, flux is transferred to the $B^{3+}(1s3d)$ and further to the $B^{3+}(1s3p)$ channel, with a probability close to unity. However, at R_3 (7.0 a.u.) the energy difference is rather large. Therefore, some portion of the flux is transferred to the $B^{3+}(1s3s)$ channel, and the rest remains in the $B^{3+}(1s3p)$ channel. On the other hand, at intermediate collision energies the flux cannot pass completely through at R_2, causing the finite transition from the $B^{3+}(1s3d)$ channel to the $B^{3+}(1s3p)$ channel. At very low collision energies, crossings at both R_2 and R_1 become effective, resulting in a finite transition probability. With regard to the trajectory effect of the heavy particles, the Coulomb trajectory underestimates the cross sections rather significantly below 50 eV/amu because of a strong repulsion that prevents a close encounter between two heavy particles, as discussed in detail in previous papers [1,2,4].

2. *Singlet manifold*

Figure 4 shows the total and partial cross sections for the singlet manifold. Recall that in the $B^{3+}(1snl, n=3$ and 4) states, the energy levels are not in the natural order (Sec. II A). Hence, the roles of the $B^{3+}(1s3p)$ and $B^{3+}(1s3d)$ states and those of the $B^{3+}(1s4p)$ and $B^{3+}(1s4f)$ states in electron capture are reversed in the triplet and singlet manifolds, respectively. The cross sections of the $B^{3+}(1s4s)$ and $B^{3+}(1s4f)$ states in the singlet manifold are larger than those for the triplet manifold at high collision energies, but they are still considerably smaller compared to those of the $B^{3+}(1s3l)$ states. At higher collision energies, above 1 keV/amu, two states [$B^{3+}(1s3p)$ and $B^{3+}(1s3d)$] contribute comparably to electron capture. At intermediate energies (1–100 eV/amu), the $B^{3+}(1s3d)$ state contributes most to electron capture. At still lower energies, below 1 eV/amu, the $B^{3+}(1s3p)$ state becomes dominant.

Except for the reversed order of two states [$B^{3+}(1s3p)$ and $B^{3+}(1s3d)$], a similar argument for electron-capture dynamics made for the triplet manifold would hold for the singlet case. At R_1 the energy difference between the initial and $B^{3+}(1s3p)$ states of the singlet manifold is larger than the corresponding energy difference between the initial and $B^{3+}(1s3d)$ states in the triplet manifold. Therefore, the cross section of the $B^{3+}(1s3p)$ state in the singlet manifold has a larger value at 0.1–100 eV/amu region than that of the $B^{3+}(1s3d)$ state in the triplet manifold. At R_2, the energy difference between the $B^{3+}(1s3p)$ and $B^{3+}(1s3d)$ states in the singlet manifold is smaller than that for the triplet manifold. Thus, the cross section of the $B^{3+}(1s3d)$ state in the singlet manifold is larger at lower collision energies than that of the $B^{3+}(1s3p)$ state in the triplet manifold.

3. *Stueckelberg oscillation*

In Fig. 4, remarkable oscillatory structures can be clearly seen in the partial (and hence the total) cross section for the $B^{3+}(1s3d)$ state at collision energies below 10 eV/amu. Careful inspection of the results suggests that the weak oscillations also appear in the $B^{3+}(1s3p)$ state of the singlet manifold; to a lesser extent, they are visible in the triplet manifold as well (in Fig. 3). To study the origin of these oscillations, we carried out a semiclassical analysis of phase shifts using relevant adiabatic potentials [16], and examined squares of the scattering matrix element as a function of partial wave l for several collision energies. We found that these structures are Stueckel-

berg oscillation. In Fig. 5, we present scattering s-matrix elements for electron capture to the $B^{3+}(1s3d)$ state of the singlet manifold [or $B^{3+}(1s3p)$ of the triplet manifold] to show differences in the cycle of increase and decrease of the s-matrix elements. [Note that the squares of the s matrix are multiplied by $(l+\frac{1}{2})/k^2$ in Fig. 5, where k is the wave number.] The four energies shown correspond to the energies that give the positions of the maximum and the minimum in the oscillations in Fig. 4.

At collision energies lower than $E=0.566$ eV/amu, only one peak appears. As the energy decreases, the position of the peak shifts to a smaller value of l with reduced height. As a result, the cross section decreases accordingly. As the collision energy increases from 0.566 to 1.19 eV/amu, the corresponding peak shifts toward a larger value of l, and the peak becomes narrower. Thus, the cross section decreases similarly on both sides of $E=0.566$ eV/amu. As the collision energy increases further from 1.19 to 2.41 eV/amu, the second smaller peak appears at smaller values of l, and thus the cross section starts to increase. A further increase in the collision energy beyond 2.41 eV/amu repeats this shift and a narrowing of the peaks, causing the cross section to decrease again. Repetition of this trend in the s-matrix results in oscillation in the cross section. For the triplet manifold shown for the $B^{3+}(1s3p)$ in Fig. 5(b), the circumstance is slightly different. The size of the corresponding peak becomes linearly larger as energy increases. Thus, the narrowing effect of the peak (that is, the decrease of the cross section) does not offset the increase in peak size. The presence of the extremum in the energy difference between relevant adiabatic potentials (see Fig. 1) and the features in the s-matrix (Fig. 5) are typical of Stueckelberg-type oscillation [16]. At high energy and in a two-state approximation, the total capture cross section can be written as $\sigma \propto (1/k^2)\sum_l (2l+1)\sin^2\delta_l$ and $\delta_l \propto (1/v)\int R\Delta V/(R^2-b^2)^{1/2}dR$, where ΔV is the potential difference between the initial and electron-captured channels, and b and R describe the impact parameter and internuclear separation, respectively. When an extremum in ΔV and, hence, in δ_l exists, the cross section can be expressed on the basis of the stationary-phase approximation as $\sigma \propto \bar{\sigma} - B\cos\delta^0$, where $\bar{\sigma}$ represents a smoothly varying cross section, and $B\cos\delta^0$ is an oscillatory term. Therefore, on the whole, oscillatory structures are still present in the integral capture cross section.

For the singlet manifold, oscillations around 1 eV/amu are weakened because of complete mixing between the $1s3p$ and $1s3d$ states (see coupling in Fig. 2), while oscillations above that energy are manifested by a single dominant component of the $1s3d$ state. For the triplet manifold, oscillations are somewhat vague, as discussed for the s matrix above. Furthermore, interference between $1s3p$ and $1s3d$ states is not clearly seen because of weaker coupling between the two.

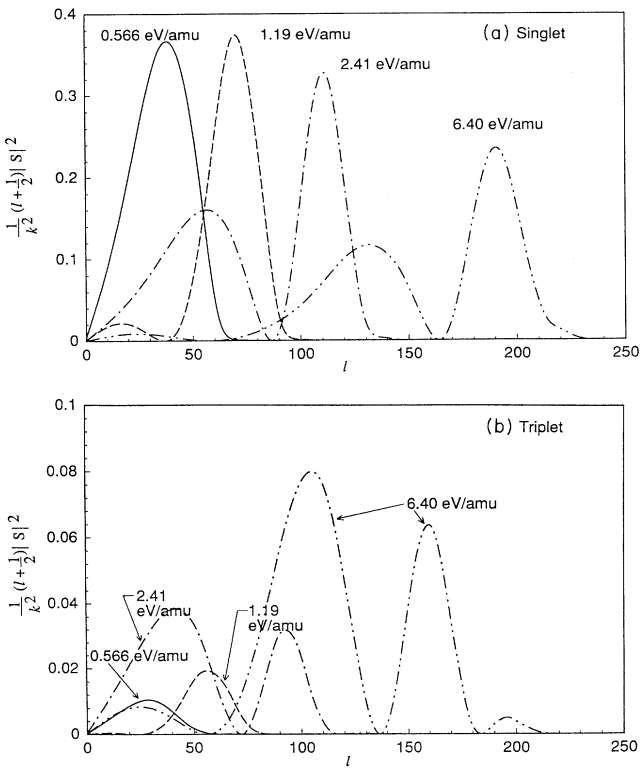

FIG. 5. Squares of the scattering matrix element as a function of the partial wave at $E=6.40$, 2.41, 1.19, and 0.566 eV/amu for (a) the singlet $B^{3+}(1s3d)$ state and (b) the triplet $B^{3+}(1s3p)$ state.

4. *Total cross sections*

Figure 6 displays the present total cross sections along with other measurements [6–8]. Our results were obtained by summing the values for the triplet and singlet manifolds with appropriate statistical weights. The experimental results scatter over a wide range, from 25×10^{-16} cm^2 at 2 keV/amu to 50×10^{-16} cm^2 at 8 keV/amu, but our results lie among these data. Our results agree very well with the measurements of Gardner *et al.* [8] at their two lowest-energy points.

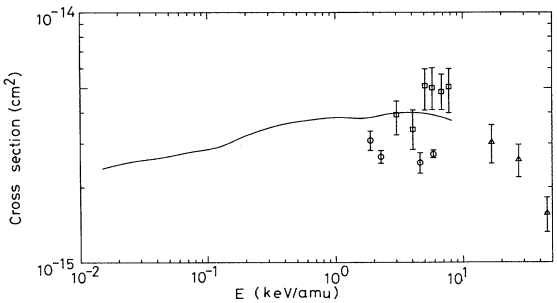

FIG. 6. Comparison of our calculated results with measurements. The solid curve represents our semiclassical results. Experiment: ○, Crandall, Phaneuf, and Meyer [6]; □, Gardner *et al.* [8]; △, Goffe, Shah, and Gilbody [7].

5. *Core-electron effect and scaling*

To examine the effect of core electrons on the capture mechanism, we plot in Fig. 7 the present total cross sections along with other "best" theoretical results for electron capture from the hydrogen atom by projectiles that have the *same effective charge of four but different numbers of core electrons.* These systems are the Be^{4+} ion (no core electron) [17,18], the B^{4+} ion (one 1*s* electron, open core), the C^{4+} ion (two 1*s* electrons, closed core) [19,20], and the N^{4+} ion (two 1*s* and one 2*s* electrons, open core) [4]. The present results for the (B^{4+} +H) system are semiquantitatively similar in both magnitude and energy dependence to those for the (N^{4+} +H) system in most of the energy regions studied. The cross sections are quite energy independent and nearly constant. Both of these are open-core systems with singlet and triplet manifolds. The cross sections for the (C^{4+} +H) and (Be^{4+} +H) systems, which are closed-core systems, show a rather sharp decrease below 1 keV/amu, although the cross section for (Be^{4+} +H) drops faster than that for (C^{4+} +H). In addition, the maximum positions in the cross sections are different. In this respect, the (C^{4+} +H) and (Be^{4+} +H) systems are rather different from the previous two systems (B^{4+} and N^{4+} with H). However, all results from the four systems appear to converge within a narrow range at energies above 1 keV/amu.

The effect of core electrons on a colliding partner is manifested by features in the adiabatic potentials for all four systems. For closed-core or no core systems, the electronic structure is rather simple because only the doublet state is possible, while both singlet and triplet manifolds are available for open-core systems. Although the locations of the avoided crossings between the initial and the dominant electron-capture channels are in nearly the same *R* region for all four systems (because of the same H target and final charge state), the features of the avoided crossings among them are more complicated in open-core systems (i.e., there is a core electron effect). Energy splitting at avoided crossings are generally somewhat wider for the closed-core systems than for the open-core systems because no strong electron mixing occurs, implying smaller capture cross sections in the former in low-energy regions.

At low energies, a captured electron has a longer interaction time, with the incoming projectile causing complex multichannel and multielectron interactions. Hence, the unique, individual character of a projectile becomes more conspicuous. This phenomenon causes different magnitudes and energy dependencies in the cross sections of different systems. As the energy increases, the collision dynamics become increasingly impulsive, and a perturbative treatment becomes valid. In this energy region, the captured electron rarely feels an effect of core electrons during the collision, and the electron-capture process is controlled mainly by the effective projectile charge, apparently giving similar magnitudes to the capture cross sections if the projectiles have the same charge. At high energy, the electron-capture cross section resulting from collisions of fully stripped ions with H atoms can be described simply as a function of projectile charge (Z_p) and velocity (v) according to the perturbation treatment. Hence, the idea of scalability of the cross section emerges, as shown by Briggs [21].

In conjunction with the ideas of (1) individual unique features of electronic states that govern collision dynamics at low energies and (2) perturbative treatment of collision dynamics at high energies, it is interesting to see how well a proposed scaled form of the cross section reproduces known cross-section data and how it deviates from those data. We have used the scaled form of the capture cross section proposed semiempirically by Ryufuku and Watanabe [22] to examine the validity and

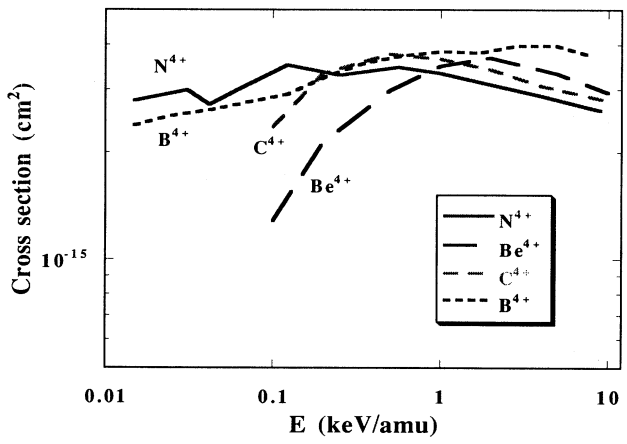

FIG. 7. Collision energy dependence of the total electron-capture cross sections of the (B^{4+} +H) system along with other theoretical results for systems with the same charge. The dotted curve represents the present semiclassical results. (N^{4+} +H) system: ——, Shimakura, Itoh, and Kimura [4]. (Be^{4+} +H) system: — — —, Fritsch and Lin [18]. (C^{4+} +H) system: --- Fritsch and Lin [19].

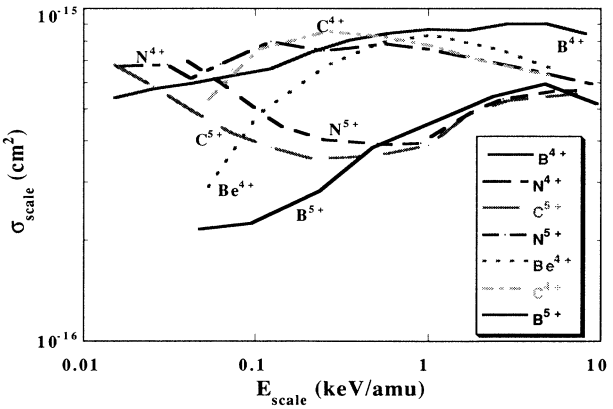

FIG. 8. Scaled cross sections σ_{scale} ($=\sigma/Z_p^{1.07}$) (cm^2) as a function of scaled collision energy E_{scale} ($=E/Z_p^{0.464}$) (keV/amu). Be^{4+}: Fritsch and Lin [18]; B^{4+}: present; C^{4+}: Fritsch and Lin [19]; N^{4+}: Shimakura, Itoh, and Kimura [4]; B^{5+}: Fritsch and Lin [18]; C^{5+}: Shimakura *et al.* [2]; N^{5+}: Shimakura and Kimura [1].

universality of the scaling rule. The scaled cross sections $\sigma_{\text{scale}}(=\sigma/Z_p^{1.07})$ are plotted in Fig. 8 as a function of the scaled collision energy $E_{\text{scale}}(=E/Z_p^{0.464})$ for the ions Be^{4+}, B^{4+}, C^{4+}, N^{4+}, B^{5+}, C^{5+}, and N^{5+}. Above the scaled energy of 10 keV/amu (not shown), all results can apparently be represented reasonably well by the universal scaled curve of Ryufuku and Watanabe. In the scaled energy regions of 0.1–10 keV/amu, the cross sections from each Z_p group seem to stay together rather closely, suggesting that a different form of the scaling might well be possible. This stepwise discreteness of the scaled cross section as a function of projectile charge (for lower Z_p) was also noted by Kaneko *et al.* [23]. Perhaps the introduction of other quantities related to the molecular nature of the system could lead to a different type of scaling that is similar to the Landau-Zener formula. Below the scaled energy ~ 0.1 keV/amu, each characteristic (of the electronic structure) of a colliding partner becomes more conspicuous. Certainly, no such scaling rule is known here. Although a scaling rule like that of Ryufuku and Watanabe is generally regarded as a representation for highly charged (or fully stripped) ion-H systems in high-energy collisions, it still offers a reasonable fit for the cross sections of the present ions with low charges. However, any comprehensive and systematic understanding of the scaling will require a more systematic collection of cross section data for a wide variety of ions over a wide range of energies. Collaborative theoretical and experimental efforts are urgently needed to achieve this goal.

ACKNOWLEDGMENTS

This work was supported in part by the U.S. Department of Energy, Office of Energy Research, Office of Health and Environmental Research, under Contract No. W-31-109-ENG-38 (M.K.); by the Office of Basic Energy Science, Division of Chemical Sciences, through Rice University (N.S.); and by the R. A. Welch Foundation (N.S.). N.S. was also supported by a Grant-in-Aid for Scientific Research from the Ministry of Education of Japan (01540312). Some portions of the present calculation were carried out at the computer centers of Tohoku University and Niigata University.

[1] N. Shimakura and M. Kimura, Phys. Rev. A **44**, 1659 (1991).
[2] N. Shimakura, S. Koizumi, S. Suzuki, and M. Kimura, Phys. Rev. A **46**, 7876 (1992).
[3] N. Shimakura, S. Suzuki, and M. Kimura (unpublished).
[4] N. Shimakura, M. Itoh, and M. Kimura, Phys. Rev. A **45**, 267 (1992).
[5] R. A. Phaneuf, R. K. Janev, H. Tawara, M. Kimura, P. S. Krstic, G. Peach, and M. A. Mazing, J. Nuclear Fusion Suppl. **3**, 105 (1992).
[6] D. H. Crandall, R. A. Phaneuf, and F. W. Meyer, Phys. Rev. A **19**, 504 (1979).
[7] T. V. Goffe, M. B. Shah, and H. B. Gilbody, J. Phys. B **12**, 3763 (1979).
[8] L. D. Gardner, J. E. Bayfield, P. M. Koch, I. A. Sellin, D. J. Pegg, R. S. Peterson, and D. H. Crandall, Phys. Rev. A **21**, 1397 (1980).
[9] M. Kimura, H. Sato, and R. E. Olson, Phys. Rev. A **28**, 2085 (1983).
[10] N. Shimakura, J. Phys. B **21**, 2485 (1988).
[11] M. Kimura and N. F. Lane, in *Advances in Atomic, Molecular, and Optical Physics,* edited by D. R. Bates and B. Bederson (Academic, New York, 1989), Vol. 26, p. 79.
[12] H. Sato, M. Kimura, A. Wetmore, and R. E. Olson, J. Phys. B **16**, 3037 (1983).
[13] S. Bashkin and J. R. Stoner, Jr., *Atomic Energy Levels and Grotorian Diagrams I* (North-Holland, Amsterdam, 1975).
[14] J. S. Sims, D. R. Parmer, and J. M. Rees, J. Phys. B **15**, 327 (1982); C. Froesse Fischer (private communication).
[15] C. E. Moore, *Atomic Energy Levels,* Natl. Bur. Stand. (U.S.) Circ. No. 467 (U.S. GPO, Washington, D.C., 1949).
[16] R. E. Olson, Phys. Rev. A **2**, 121 (1970).
[17] K. Wada and T. Murai, J. Phys. B **18**, 4259 (1985).
[18] W. Fritsch and C. D. Lin, Phys. Rev. A **29**, 3039 (1984).
[19] W. Fritsch and C. D. Lin, J. Phys. B **17**, 3271 (1984).
[20] M. Gargaud, R. McCarroll, and P. Valiron, J. Phys. B **20**, 1555 (1987).
[21] J. Briggs, Rep. Prog. Phys. **39**, 217 (1976).
[22] H. Ryufuku and T. Watanabe, Phys. Rev. A **20**, 1828 (1979).
[23] Y. Kaneko, T. Iwai, S. Ohtani, K. Okuno, N. Kobayashi, S. Tsurubuchi, M. Kimura, H. Tawara, and S. Takagi, in *Physics of Electronic and Atomic Collisions,* edited by S. Datz (North-Holland, Amsterdam, 1982), p. 697.